Transition state mimics are valuable mechanistic probes for structural studies with the arginine methyltransferase CARM1

Matthijs J. van Haren[a,1], Nils Marechal[b,1], Nathalie Troffer-Charlier[b], Agostino Cianciulli[c], Gianluca Sbardella[c], Jean Cavarelli[b,2], and Nathaniel I. Martin[a,2]

[a]Department of Chemical Biology & Drug Discovery, Utrecht Institute for Pharmaceutical Sciences, Utrecht University, 3584 CG Utrecht, The Netherlands; [b]Department of Integrated Structural Biology, Institut de Génétique et de Biologie Moléculaire et Cellulaire, Université de Strasbourg, CNRS UMR 7104, INSERM U 964, Illkirch, F-67404, France; and [c]Epigenetic Med Chem Lab, Dipartimento di Farmacia, Università degli Studi di Salerno, I-84084 Fisciano (SA), Italy

Edited by Jocelyn Côté, University of Ottawa, Ottawa, Canada, and accepted by Editorial Board Member Gregory A. Petsko February 28, 2017 (received for review November 6, 2016)

Coactivator associated arginine methyltransferase 1 (CARM1) is a member of the protein arginine methyltransferase (PRMT) family and methylates a range of proteins in eukaryotic cells. Overexpression of CARM1 is implicated in a number of cancers, and it is therefore seen as a potential therapeutic target. Peptide sequences derived from the well-defined CARM1 substrate poly(A)-binding protein 1 (PABP1) were covalently linked to an adenosine moiety as in the AdoMet cofactor to generate transition state mimics. These constructs were found to be potent CARM1 inhibitors and also formed stable complexes with the enzyme. High-resolution crystal structures of CARM1 in complex with these compounds confirm a mode of binding that is indeed reflective of the transition state at the CARM1 active site. Given the transient nature of PRMT–substrate complexes, such transition state mimics represent valuable chemical tools for structural studies aimed at deciphering the regulation of arginine methylation mediated by the family of arginine methyltransferases.

protein arginine *N*-methyltransferase | PRMT | CARM1 | transition state mimics | cocrystal structures

The methylation of arginine residues by protein arginine *N*-methyltransferases (PRMTs) plays a vital role in a variety of key cellular functions including gene regulation, signal transduction, RNA processing, and DNA repair (1, 2). Conversely, dysregulated PRMT activity is known to be linked to a variety of cancers and other diseases (3, 4). Coactivator associated arginine methyltransferase 1 (CARM1, also known as PRMT4) is directly involved in numerous cellular processes via methylation of the histone H3 tail peptide, splicing factors, RNA binding proteins, and coactivation of nuclear receptors (1, 5). Growing evidence indicates associations with the up-regulation of CARM1 in breast (6, 7), colon (8, 9), prostate (9, 10), and liver (11) cancers, making it an appealing potential therapeutic target.

Like all lysine and arginine methyltransferases, CARM1 uses the cofactor *S*-adenosine-L-methionine (AdoMet) as the source of the methyl group that is transferred to the guanidine group of the arginine side chain in a target protein or peptide with concomitant generation of *S*-adenosine-L-homocysteine (AdoHcy) (1). As for all type 1 PRMTs, the first methylation step catalyzed by CARM1 gives monomethyl-arginine (MMA), followed by a second methylation to form asymmetric dimethyl-arginine (aDMA). Although the different PRMTs vary significantly in overall size and sequence, they share a common active site architecture defined by specific amino acids (belonging to the so-called motifs I to IV) known to be key for catalysis (Fig. 1*A*) (1–4, 12). Most notable in this regard are residues involved in hydrogen bonding to the adenosine moiety of AdoMet and two conserved glutamate residues that form the so-called "double-E loop" critical for chelating and orienting the guanidine group of the target arginine residue. In doing so, the target guanidine moiety is precisely presented to the electrophilic methylsulfonium group of AdoMet, facilitating an "S_N2-like" substitution reaction.

Recently, we reported a series of small molecule PRMT inhibitors wherein a guanidine moiety was covalently linked to an adenosine group meant to mimic that of AdoMet (13). Interestingly, some of these inhibitors displayed potent and specific inhibition of CARM1 with IC_{50} values in the nanomolar range (13). As a means of enhancing CARM1 selectivity, we report here an approach wherein known CARM1 substrate peptides are covalently tethered to an adenosine unit to create transition state mimics of the CARM1 methylation reaction (Fig. 1*B*). Such transition state mimics were also envisioned to serve as mechanistic probes and chemical tools for structural studies. Previous reports have highlighted the challenges associated with cocrystallizing PRMTs with their various peptide substrates (14–18). Because of these challenges, a complete structural understanding of how PRMTs achieve specificity in arginine methylation at different target sites remains elusive. Furthermore, although structures of isolated PRMTs have been published, few studies exist that provide an atomic-level characterization of the

Significance

The posttranslational methylation of arginine is a widespread epigenetic modification catalyzed by the family of protein arginine methyltransferases (PRMTs). Dysregulation of PRMT expression is implicated in the pathogenesis of many diseases including human cancers. An atomic-scale understanding of the PRMT catalytic mechanism is crucial for both fundamental biological and pharmacological applications. Despite intense efforts, crystal structures of PRMT complexes with long peptides and full-length substrates have not been solved because of their inherent instability. To address this issue, we describe peptide-based transition state mimics that form stable complexes with the PRMT enzyme coactivator associated arginine methyltransferase 1 resulting in high-resolution cocrystal structures. Our findings provide an exciting approach to understanding PRMT substrate recognition and the regulation of arginine methylation.

Author contributions: G.S., J.C., and N.I.M. designed research; M.J.v.H., N.M., N.T.-C., and A.C. performed research; M.J.v.H., N.M., N.T.-C., A.C., J.C., and N.I.M. analyzed data; and M.J.v.H., G.S., J.C., and N.I.M. wrote the paper.

The authors declare no conflict of interest.

This article is a PNAS Direct Submission. J.C. is a guest editor invited by the Editorial Board.

Data deposition: The atomic coordinates and structure factors have been deposited in the Protein Data Bank, www.pdb.org (PDB ID codes 5LGP–5LGS).

[1]M.J.v.H. and N.M. contributed equally to this work.

[2]To whom correspondence may be addressed. Email: n.i.martin@uu.nl or cava@igbmc.fr.

This article contains supporting information online at www.pnas.org/lookup/suppl/doi:10.1073/pnas.1618401114/-/DCSupplemental.

BIOCHEMISTRY

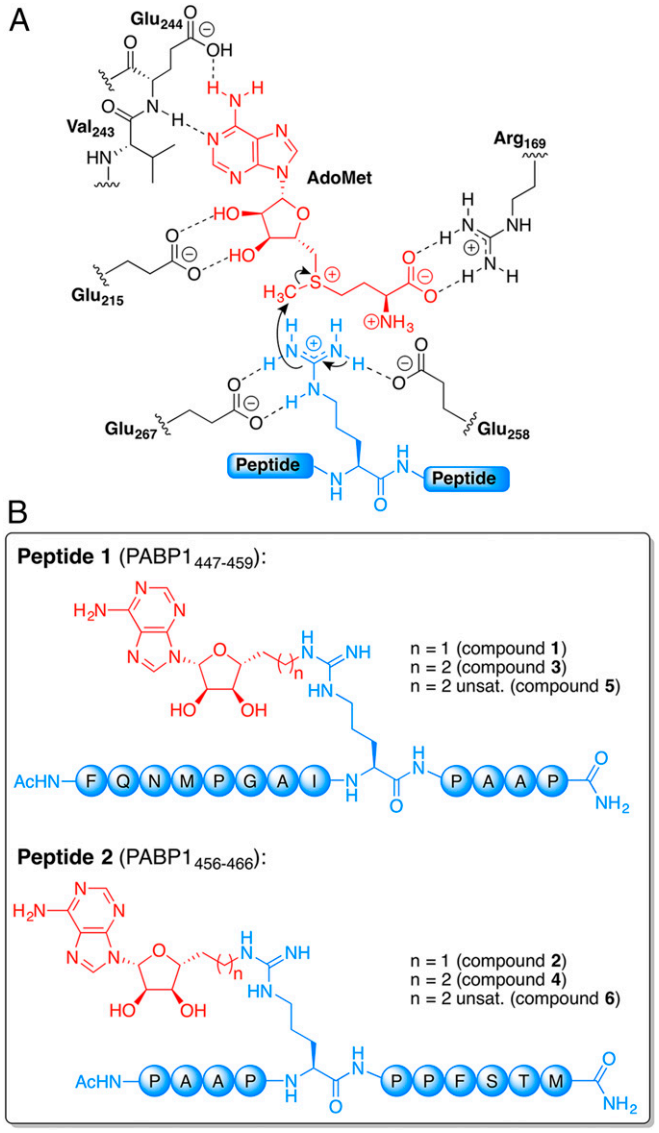

Fig. 1. The CARM1 active site and design of transition state mimics. (*A*) CARM1 employs an "S_N2-like" bisubstrate mechanism. Key active site residues are indicated including the conserved Glu_{267} and Glu_{258} residues comprising the guanidine-binding "double-E loop" (*Mus musculus* CARM1 numbering scheme). The AdoMet cofactor is highlighted in red and the target arginine-containing peptide in blue. (*B*) Structures of PABP1-derived constructs prepared in this study as CARM1 transition state mimics.

functional macromolecular complexes formed between PRMTs and their targets. Importantly, the transition-state mimicking compounds we here describe were found to cocrystallize with CARM1, forming stable complexes suitable for structural studies.

Results

Design of Transition State Mimics and Inhibition Studies. In selecting the CARM1-specific peptide substrates to be used in designing the transition state mimics, we focused on the nonhistonic poly (A)-binding protein 1 (PABP1), one of the most highly methylated CARM1 targets. Previous studies using peptide fragments derived from PABP1 identified the strongest CARM1 methylation sites as R455 and R460 (19). We therefore selected two PABP1 fragments, comprised of residues 447–459 and 456–466 (each containing a single arginine) to serve as the peptide segment of the transition state mimics (Fig. 1*B*). Building on methodology recently developed in our group (20–22), we here report a convenient on-resin approach for preparing peptides in which an adenosine group can be covalently linked to the guanidine moiety of a specific arginine residue (compounds **1–6**; Fig. 1*B*, see *SI Appendix, Materials and Methods* for complete synthetic details). Spacer lengths of two and three carbon atoms were explored because previous investigations indicated these closest mimic the PRMT transition state (13). In addition, unsaturated analogs of the three-carbon spacer constructs were also prepared to examine the effect of reduced linker flexibility. Compounds **1–6** were specifically designed so as to mimic the transition state of the first methylation reaction catalyzed by CARM1. Given that the first catalytic step is common to all PRMTs, this strategy represents a general approach that should be applicable for studying substrate binding by any PRMT enzyme (type I, II, or III) and its corresponding substrate(s). Also prepared were compounds **7** and **8**, in which the target arginine of the PABP1 fragments was incorporated as the asymmetrically dimethylated species. Compounds **7** and **8** thus represent product inhibitors of CARM1 and were included as a means of evaluating the relative inhibitory potency of transition state mimics **1–6**.

The inhibitory activity of compounds **1–8** toward CARM1 was investigated and compared with the ability to inhibit PRMT1, the most abundant arginine methyltransferase. An initial inhibition screen performed at a fixed inhibitor concentration of 50 μM revealed that compounds **1–6** were all effective CARM1 inhibitors, whereas the dimethylated PABP1-derived peptides **7** and **8** showed no effect under these conditions. Based on these preliminary findings, complete IC_{50} curves were generated for compounds **1–6** against both CARM1 and PRMT1 (Table 1). Analogs containing three-atom saturated linkers (compounds **3** and **4**) and unsaturated linkers (compounds **5** and **6**) display the most potent inhibition of CARM1 with IC_{50} values <100 nM. Shortening the spacer from three to two carbon atoms results in a significant decrease in activity, suggesting that a three-atom linker between the guanidine moiety and the adenosine group is optimal for mimicking the transition state geometry. When tested against PRMT1, compounds **1–6** displayed significantly reduced inhibitory activity. In light of these findings, we next examined the application of the more potent CARM1 inhibiting compounds **3–6** as transition state mimics for use in cocrystallization studies.

Crystallization and Structure Determination of CARM1 Complexes with Transition State Mimicking Compounds 3–6. Cocrystallization studies were performed with the PABP1-derived transition state mimics and an isolated catalytic domain of mm*CARM1* (*Mus musculus CARM1*, residues 130–487) (15, 23). All structures

Table 1. IC_{50} values measured for compounds 1–8 against CARM1 and PRMT1

Compound	IC_{50} values*	
	CARM1	PRMT1
AdoHcy	0.276 ± 0.052	7.65 ± 2.98
1 (Peptide 1, *n* = 1)	1.93 ± 0.55	16.28 ± 4.49
2 (Peptide 2, *n* = 1)	5.90 ± 0.87	16.29 ± 5.68
3 (Peptide 1, *n* = 2)	0.0920 ± 0.0132	12.34 ± 3.65
4 (Peptide 2, *n* = 2)	0.0901 ± 0.0107	25.54 ± 7.40
5 (Peptide 1, *n* = 2, unsat.)	0.0817 ± 0.0116	4.29 ± 1.04
6 (Peptide 2, *n* = 2, unsat.)	0.0876 ± 0.0092	16.62 ± 5.96
7 (Peptide 1, aDMA)†	>50	>50
8 (Peptide 2, aDMA)†	>50	>50

*IC_{50} values reported in micromolars. IC_{50} values from triplicate data obtained at a range of 7–10 concentrations ± SD (see *SI Appendix, IC_{50} curves*).
†In compounds **7** and **8**, the central arginine residue is present in asymmetrically dimethylated form.

were solved and refined to 2-Å resolution in the space group $P2_12_12$ as seen for mmCARM1 catalytic domain (15) and contain one copy of the CARM1 tetramer in the asymmetric unit (*SI Appendix*, Table S1). In all cases, each CARM1 monomer binds one molecule of the transition state mimic investigated (Fig. 2*A*). As indicated in Fig. 2*B*, the structures solved include near-complete assignment of all residues in the peptide fragments of compounds **3–6**. Compounds **3** and **5** are comprised of a 13-aa sequence from PABP1 (residues 447–459) centered around R455, flanked by eight residues on the N-terminal side and four residues on the C-terminal side. The electron density maps obtained in the cocrystallization studies with both **3** and **5** reveal the conformation of 12 of 13 residues in two monomers and for the full-length peptide (13 residues) in the two other CARM1 monomers (Fig. 3*A*). Compounds **4** and **6** are comprised of an 11-aa sequence from PABP1 (residues 456–466) centered around R460 flanked by four residues on the N-terminal side and six residues on the C-terminal side. The electron density maps obtained in the cocrystallization studies with both **4** and **6** reveal the conformation of 8 of 11 residues in three of the monomers and 9 of 11 residues in the remaining CARM1 monomer (Fig. 3*B*). The last two residues on the C-terminal side of **4** and **6** are not seen in the electron density map. As expected for the structures obtained with compounds **3–6**, the adenosine moiety occupies the AdoMet binding pocket. In the other CARM1 structures reported to date, this same pocket is occupied by either AdoHcy or sinefungin (15–18).

The three carbon-atom linker appears to provide the ideal spacer to position and orient both the adenosine group and the modified arginine residue present in the peptide-based transition state mimics (Fig. 4). Specifically, the four PRMT signature motifs surround the binding pocket occupied by the covalently linked adenosine and arginine components of compounds **3–6**. The catalytic site is locked on one side by the PRMT motif I ($Y_{150}F_{151}xxY_{154}$ mmCARM1 numbering) and the guanidine moiety of the arginine side chain is hydrogen-bonded to E258 and E267 belonging to the double-E loop and H415 of the THW loop. Of particular interest is the comparison of the binding modes for the transition state mimics that contain a fully saturated spacer (**3** and **4**) with those containing an unsaturated spacer (**5** and **6**), revealing both to have similar conformations (Fig. 4 and *SI Appendix*, Figs. S3 and S4). These findings indicate that the unsaturated spacers in **5** and **6** lead to a preformed conformation suitable for binding in the CARM1 active site. The additional hydrogen atoms present in the saturated linkers of compounds **3** and **4** result in a modification of the conformation of M269 and a slightly different network of water molecules (Fig. 4 and *SI Appendix*, Fig. S3).

Another striking result is the finding that the conformations observed for the peptide components of the CARM1-bound

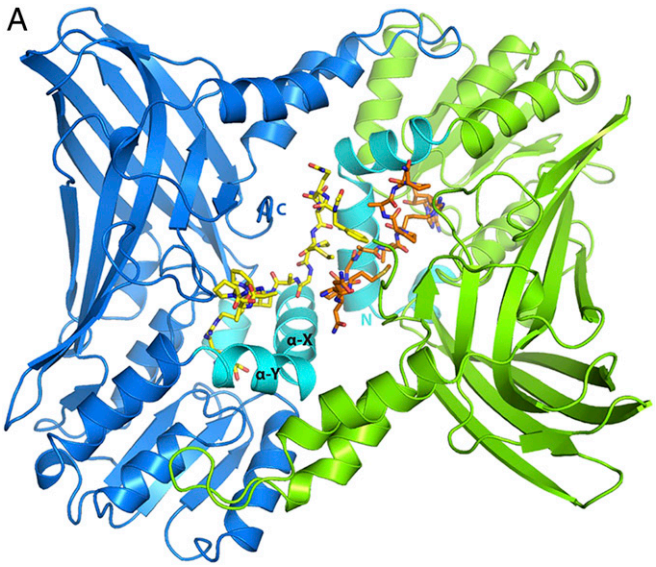

Fig. 2. Crystallization and structure determination of CARM1-transition state mimic complexes. (*A*) Dimer of mmCARM1 with compound **3** bound. CARM1 monomers within the dimer (green, blue) are represented as a cartoon. Compound **3** is represented as sticks. N-terminal helices of each monomer (not shown in other figures) are here highlighted in light blue. (*B*) Peptides sequences used and results from crystallization studies with compounds **3–6**: Residues visible in all four monomers of the asymmetric unit indicated in green and those seen in at least one monomer are shown in red. Compounds **3** and **4** contain a saturated three-atom spacer, whereas compounds **5** and **6** contain an unsaturated three-atom spacer.

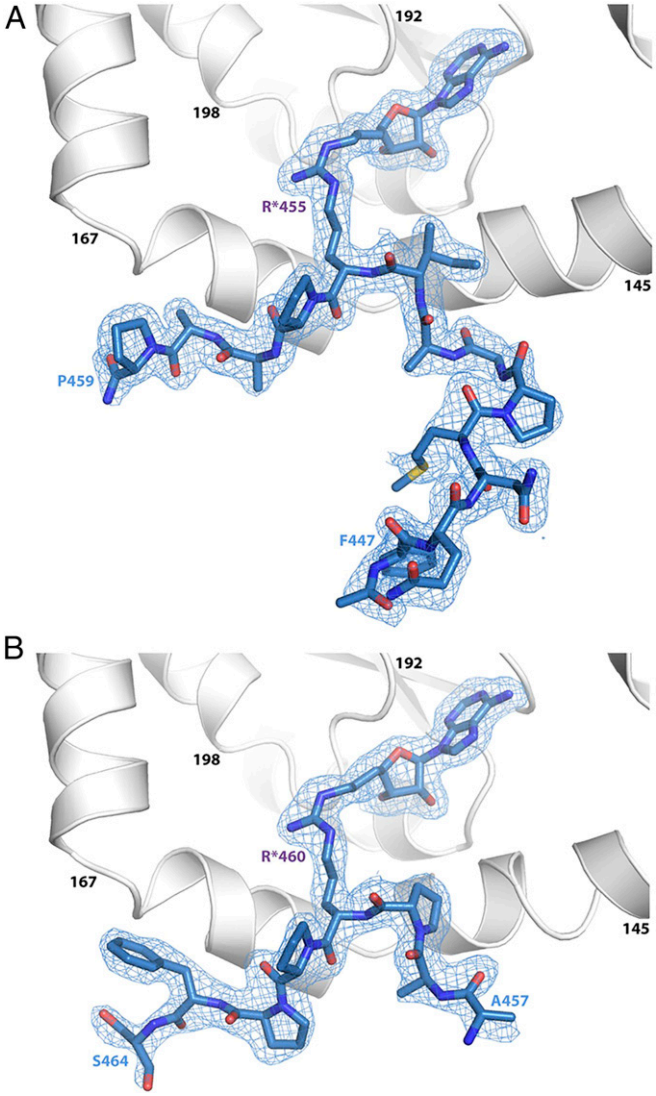

Fig. 3. Electron density ($2F_{obs}-F_{calc}$) weighted maps. Compound **5** (*A*) and compound **6** (*B*) bound to subunit B of mmCARM1. CARM1 is represented as cartoon, and peptide-based transition state mimics **5** and **6** are represented as sticks. Maps are represented as a mesh, contouring level set to 1σ.

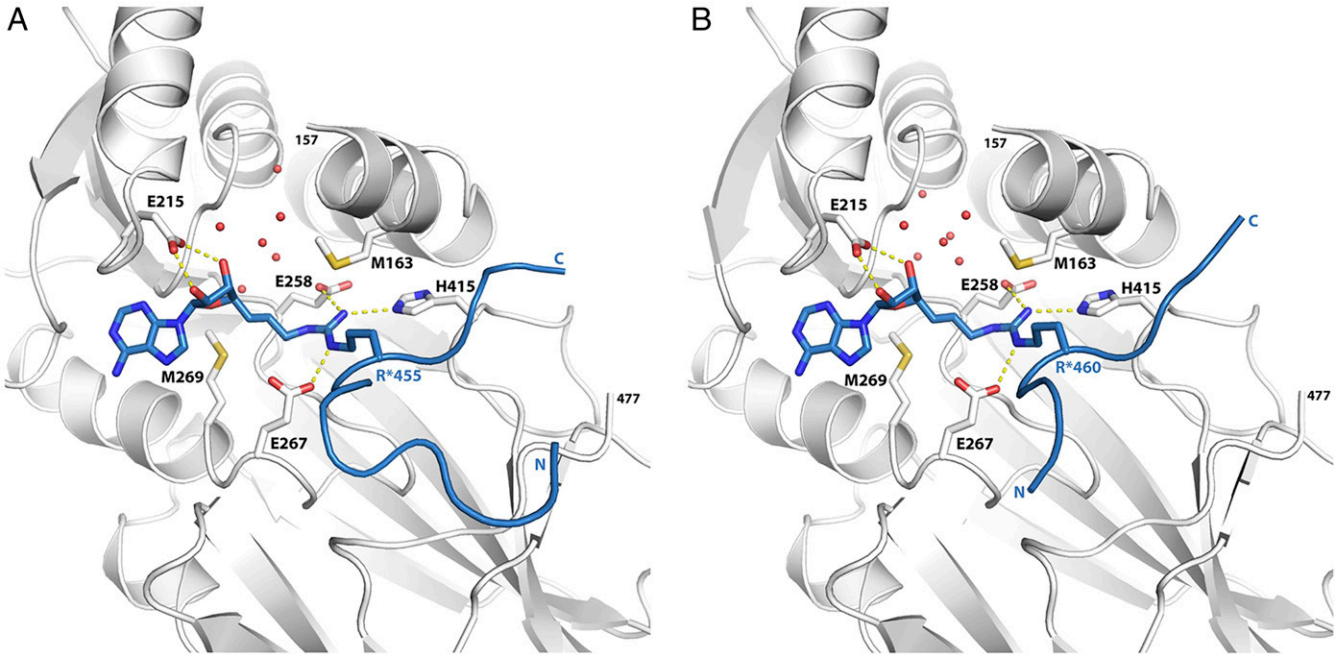

Fig. 4. Cocrystal structures of CARM1 with transition state mimics **5** and **6** revealing interacting active site residues and water molecules. Cartoon and stick representation of the transition state mimics bound to mmCARM1. Compound **5** is derived from $PABP1_{447–459}$ (*A*) and compound **6** is derived from $PABP1_{456–466}$ (*B*). Both compounds contain an unsaturated linker between the guanidine moiety and the adenosine unit. For clarity, N-terminal helices of CARM1 are not shown.

transition state mimics are identical to those observed with unmodified PABP1 fragments bound to CARM1 in a recently reported cocrystallization study (18). Superimposition of the structures of the binary complexes formed between mmCARM1 and transition state mimics **3** or **5** with the structures recently reported for the ternary complexes of hsCARM1, sinefungin, and a PABP1-derived peptide containing R455 (18) reveal an identical conformation for the visible PAPB1 substrate peptide in both complexes (Fig. 5*A* and *SI Appendix*, Figs. S5 and S6). A similar result is obtained when superimposing the structures of binary complexes of mmCARM1 and transition state mimics **4** and **6** with the ternary complex of hsCARM1, sinefungin, and another PABP1-derived peptide containing R460 (Fig. 5*B* and *SI Appendix*, Fig. S6). Moreover, the electron density maps of the complexes of mmCARM1 with **3** and **5** reveal the conformation of four more residues at the N-terminal side of the peptide compared with the ternary complexes of hsCARM1, sinefungin, and the PABP1-derived peptide containing R455 (Fig. 5*A* and *SI Appendix*, Fig. S5). In the case of the complexes formed between mmCARM1 and transition state mimics **4** and **6**, two additional N-terminal residues are also visible compared with the ternary complex of hsCARM1, sinefungin, and a PABP1-derived peptide containing R460 (Fig. 5*B* and *SI Appendix*, Fig. S6). Furthermore, it is interesting to note that the recently reported hsCARM1-PABP1 peptide complexes could only be solved in the presence of the AdoMet-competitive methyltransferase inhibitor sinefungin (18). The inclusion of sinefungin in the AdoMet binding site has an impact on the conformation of R169 that normally interacts with the methionine moiety of AdoMet. This distortion in turn leads to a small alteration in the conformation of E258, resulting in a change in the arrangement of bound water molecules. By comparison, transition state mimics **3–6** do not introduce such disturbances in the active site. The three carbon-atom linker used in these conjugates serves to properly orient and position the substrate peptide while simultaneously docking the adenosine moiety in the AdoMet binding site. In doing so, a "frozen" image of the transition state of the methylation reaction is effectively achieved.

Discussion

Given the challenges associated with obtaining stable complexes of PRMTs and their corresponding protein substrates, the majority of PRMT crystal structures reported to date are of free enzyme, often bound to an analog of the AdoMet cofactor. These structures reveal a strong conservation of catalytic domain architecture and specifically the AdoMet binding pocket. In contrast, no structures have been solved for PRMTs in complex with full-length target proteins, and only a few structures have been reported for PRMTs in complex with small, well-resolved, peptide substrate fragments (18, 24, 25). The covalent tethering of substrates to enzymes has proven to be an effective strategy for capturing difficult to characterize enzyme–substrate complexes, leading to their structural characterization (26, 27). In a related approach, we describe here the application of transition state mimics for enabling structural studies with the PRMTs. Specifically, we designed transition state mimics **1–6** based on CARM1 peptide substrates wherein the arginine that is normally methylated is instead covalently linked to an adenosine moiety mimicking that present in the AdoMet cofactor. Compounds **3–6** were found to be particularly potent inhibitors of CARM1, and the subsequently solved cocrystal structures reveal that they are effective transition-state mimics capable of revealing biologically relevant peptide conformations. This assertion is supported by the near-identical conformations seen when superimposing the binary complexes described here with the recently reported ternary structures of hsCARM1, sinefungin, and a PABP1-derived peptide (18). Furthermore, it is interesting to note that ternary hsCARM1–PABP1 peptide complexes could only be solved in the presence of the AdoMet-competitive methyltransferase inhibitor sinefungin. The inclusion of sinefungin in the AdoMet binding site has an impact on the conformation of several residues. By comparison, the transition state mimics here described do not introduce any unnatural perturbations of the AdoMet binding site.

It has been shown that long distance interactions are crucial for substrate recognition and binding by PRMTs (15–18, 28, 29). However, despite extensive efforts, crystal structures of PRMT

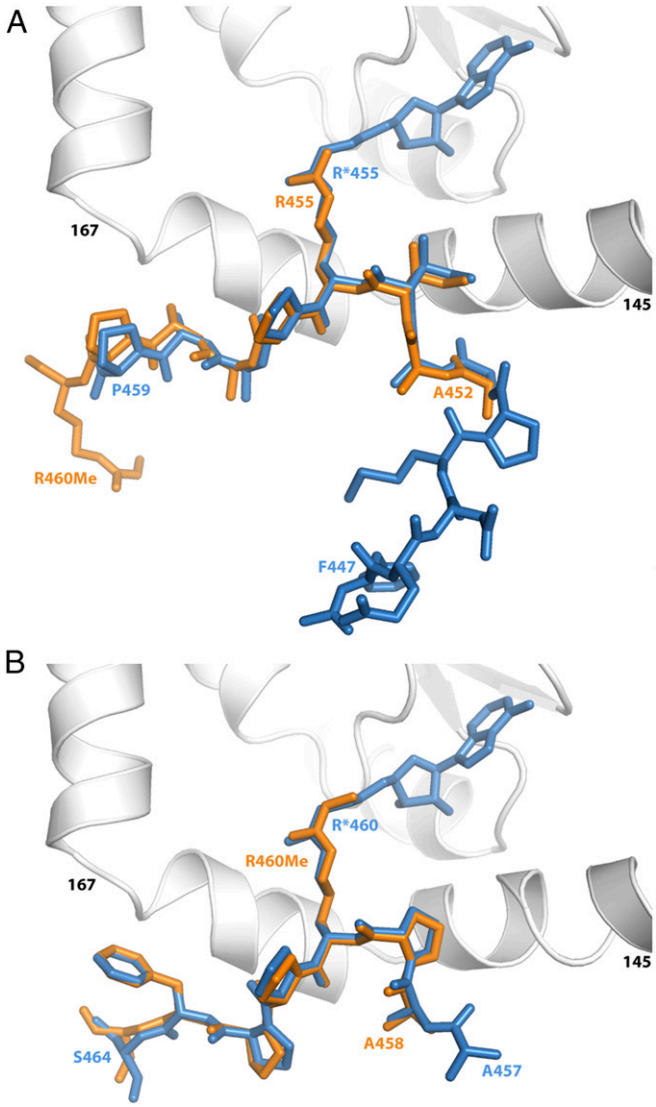

Fig. 5. Structures of transition state mimics overlaid with isolated peptides in presence of SFG. Superimposition of transition state analogs **5** and **6** and free PABP1 peptides on CARM1. (*A*) Superimposition of compound **5** (blue sticks) bound to mmCARM1 on SFG-PABP1(R455) (orange sticks) bound to hsCARM1 (PDB ID code 5DX1). (*B*) Superimposition of compound **6** (blue sticks) bound to mmCARM1 on SFG-PABP1(R460-MMA) (orange sticks) bound to hsCARM1 (PDB ID code 5DXA). SFG molecule is not shown for the hsCARM1 structures.

complexes with longer peptides or full-length substrates have not yet been solved. The transition state mimic approach here described presents a strategy toward stabilizing PRMT–substrate complexes for use in structural studies aimed at deciphering substrate recognition and binding by PRMTs at the atomic level. The specific peptide constructs used exhibit potent CARM1 inhibition and effectively bind to the enzyme despite having limited secondary structure relative to what would be expected for full-length substrates. In this regard, the transition state mimic approach is also expected to be applicable in preparing much larger constructs (i.e., via protein total synthesis using native chemical ligation strategies) as a means of stabilizing PRMT–substrate complexes in their biologically relevant conformations. The aim of the present study was to generate transition state mimics of the first methylation reaction catalyzed by CARM1 and represents an approach that should be generally applicable to all PRMTs. It is conceivable that similar transition state mimics, bearing an additional methyl group on the guanidine unit of the modified arginine, might also be able to provide subtype-specific structural insights into PRMT catalysis. Specifically, incorporation of a methyl group at the nitrogen atom connected to the adenosine moiety could provide a transition state mimic for characterizing the active site features leading to asymmetric arginine dimethylation as for the type I PRMTs. Conversely, a mimic bearing a methyl group at the other terminal guanidine nitrogen, not connected to the adenosine group, would provide a tool with which to study symmetric dimethylation as catalyzed by the type II PRMTs.

Given the transient nature of complexes formed between PRMTs and their peptide/protein substrates, tool compounds like those presented here are expected to be of great value in achieving a comprehensive structural understanding of how PRMT methylation is regulated, an important and outstanding challenge in the field of epigenetics. In addition, insights gleaned from the approaches described here may also provide inspiration for the design of smaller, peptidomimetic compounds that retain the potent and selective bisubstrate inhibitory properties of the transition state mimics.

Materials and Methods

Synthetic Procedures. Compounds **1–8** were synthesized by using a newly developed methodology allowing for the on-resin preparation of peptides containing N^G-substituted arginine residues. Specifically, PABP1-derived peptides were synthesized by using standard solid-phase techniques after which the adenosine group was introduced. Detailed synthetic protocols are provided in the accompanying *SI Appendix, Materials and Methods*, including experimental procedures and analytical data for all new compounds.

Enzyme Assays. Methyltransferase inhibition assays were performed as described (30) by using commercially available chemiluminescent assay kits for PRMT1 and PRMT4/CARM1 (purchased from BPS Bioscience). The enzymatic reactions were conducted in triplicate at room temperature for 1 h in substrate-coated well plates at a final reaction volume of 50 μL containing the manufacturer's proprietary assay buffer, AdoMet (at a concentration of 5 times the respective K_m value for each enzyme), the methyltransferase enzyme: PRMT1 (80 ng per reaction, final enzyme concentration 38 nM) and CARM1 (200 ng per reaction, final enzyme concentration 63 nM), inhibitors **1–6**, and AdoHcy (in the range of concentrations: 0.001–250 μM in water). Before addition of the AdoMet, the enzyme was first incubated with the inhibitor for 15 min at 37 °C. Positive controls were performed in the absence of inhibitors by using water to keep the final volume consistent. Blanks and substrate controls were performed in the absence of the enzyme and AdoMet, respectively. Following the enzymatic reactions, 100 μL of primary antibody (recognizing the respective immobilized asymmetrically dimethylated arginine product) was added to each well, and the plate was incubated at room temperature for an additional 1 h. Then, 100 μL of secondary horseradish peroxidase (HRP)-conjugated antibody was added to each well, and the plate was incubated at room temperature for additional 30 min. Finally, 100 μL of an HRP substrate mixture was added to the wells, and the luminescence was measured directly by using a standard microplate reader. In all cases, enzyme activity measurements were performed in triplicate at each of the inhibitor concentrations evaluated. The luminescence data were analyzed by using GraphPad Prism (version 6.02).

The luminescence data were normalized with the highest value obtained in a concentration range defined as 100% activity and the lowest value defined as 0%. Blank and positive controls were performed to analyze the validity of the assay method. Blank values obtained were 0.4–2.2% for PRMT1 and 4.3–29.3% for CARM1. Because the blank values were generally higher than the lowest value obtained in a concentration range, the lowest value in each series was set at 0%. Positive controls were generally within ±15% of the highest values obtained in a concentration range, but occasionally the highest values were up to 33% higher than the positive control. The percent activity values were plotted as a function of inhibitor concentrations and fitted by using nonlinear regression analysis of the Sigmoidal dose–response curve generated by using normalized data and a variable slope following Eq. **1**,

$$Y = \frac{100}{\left(1 + 10^{\left(\left(LogIC50 - X\right) * HillSlope\right)}\right)}, \quad [1]$$

where Y = percent activity, X = the logarithmic concentration of the compound, and Hill Slope = slope factor or Hill coefficient. The IC_{50} value was determined by the concentration resulting in a half-maximal percent activity. The IC_{50} values measured for AdoHcy, which served as a reference compound, are similar to those reported (13). Full IC_{50} curves are presented in *SI Appendix, IC_{50} curves*.

CARM1 Cloning, Expression, and Purification. The *Mus musculus* CARM1 gene sequence corresponding to the PRMT core (residues 130–487, mmCARM1$_{130–487}$) was amplified by PCR from the original GST-CARM1 construct (15, 31) (see *SI Appendix, Materials and Methods* for full experimental details).

X-Ray Data Collection and Structure Determination.

Crystallization. Transition state mimics **3–6** were solubilized in water before addition to the protein solution (2 mg·mL^{-1}) at the final concentration of 2 mM. The protein–peptide solution was incubated 20 min at room temperature before use. Vapor diffusion method using hanging drop trays with a 0.5-mL reservoir was used for crystallization. Typically, 2 μL of protein-ligand solution were added to 1 μL of well solution consisting of 14–16% (*v/v*) PEG 3350, 100 mM Tris·HCl pH 8.5, and 200 mM $(NH_4)_2SO_4$. Crystals grew in a few days at 293 K.

Data collection and structure solution. Crystals were flash-frozen in liquid nitrogen after a brief transfer to 5-μL reservoir solution containing 15% (vol/vol) PEG 400 as a cryoprotectant and were stored in liquid nitrogen. The diffraction datasets were collected on the SOLEIL PROXIMA1 and ESRF ID-29 beamlines, using a PILATUS 6M (Dectris) or a Quantum 315 (ADSC) detector and processed with XDS (32) and HKL-2000 (33). The crystals belonged to the $P2_12_12$ space group with four monomers of CARM1 in the asymmetric unit. The structures were solved by molecular replacement using CARM1 structure as a probe (15). Model building and refinement were carried out by using Coot (34) and PHENIX (35). TLS refinement with three groups per polypeptide chain was used. All other crystallographic calculations were carried out with the CCP4 package (36). Structure figures were generated with PyMol.

Data availability. All structures and structure factors have been deposited in the Protein Data Bank (CARM1-Compound **3** = 5LGP; CARM1-Compound **4** = 5LGQ; CARM1-Compound **5** = 5LGR; CARM1-Compound **6** = 5LGS).

Additional information. Supplementary information, chemical compound information, and source data are available in *SI Appendix, Materials and Methods*.

ACKNOWLEDGMENTS. We thank Javier Sastre Toraño for high-resolution mass spectrometry analysis, the members of the Institut de Génétique et de Biologie Moléculaire et Cellulaire (IGBMC) common services, and the members of the structural biology platform of IGBMC for technical assistance; Vincent Cura and Luc Bonnefond for help in the structural studies, and members of SOLEIL Proxima1 beamlines and the European Synchrotron Radiation Facility–European Molecular Biology Laboratory joint Structural Biology groups for the use of beamline facilities and for assistance during X-ray data collection. Financial support provided by Utrecht University and the Netherlands Organization for Scientific Research is acknowledged (M.J.v.H. and N.I.M.). J.C., N.M., and N.T-C. are supported by grants from CNRS; Université de Strasbourg; INSERM; Instruct, part of the European Strategy Forum on Research Infrastructures supported by national member subscriptions and the French Infrastructure for Integrated Structural Biology (ANR-10-INSB-05-01); Grant ANR-10-LABX-0030-INRT, a French State fund managed by the Agence Nationale de la Recherche under the frame program Investissements d'Avenir labeled ANR-10-IDEX-0002-02 and Association pour la Recherche contre le Cancer Grant SFI20121205902. G.S. is supported by grants from the Italian Ministero dell' Istruzione, dell' Università e della Ricerca (MIUR), Progetti di Ricerca di Interesse Nazionale (PRIN) Grants 2012ZHN9YH and 20152TE5PK, and from the Università di Salerno (Italy). G.S. and N.I.M. are supported by European Cooperation in Science and Technology (COST, Action CM1406). A.C. was supported by a Short-Term Scientific Mission Grant from the COST Action CM1406.

1. Fuhrmann J, Clancy KW, Thompson PR (2015) Chemical biology of protein arginine modifications in epigenetic regulation. *Chem Rev* 115:5413–5461.
2. Bedford MT, Clarke SG (2009) Protein arginine methylation in mammals: Who, what, and why. *Mol Cell* 33:1–13.
3. Yang Y, Bedford MT (2013) Protein arginine methyltransferases and cancer. *Nat Rev Cancer* 13:37–50.
4. Cha B, Jho EH (2012) Protein arginine methyltransferases (PRMTs) as therapeutic targets. *Expert Opin Ther Targets* 16:651–664.
5. Wei H, Mundade R, Lange KC, Lu T (2014) Protein arginine methylation of non-histone proteins and its role in diseases. *Cell Cycle* 13:32–41.
6. Morettin A, Baldwin RM, Côté J (2015) Arginine methyltransferases as novel therapeutic targets for breast cancer. *Mutagenesis* 30:177–189.
7. Cheng H, et al. (2013) Overexpression of CARM1 in breast cancer is correlated with poorly characterized clinicopathologic parameters and molecular subtypes. *Diagn Pathol* 8:129.
8. Ou CY, et al. (2011) A coactivator role of CARM1 in the dysregulation of β-catenin activity in colorectal cancer cell growth and gene expression. *Mol Cancer Res* 9:660–670.
9. Kim YR, et al. (2010) Differential CARM1 expression in prostate and colorectal cancers. *BMC Cancer* 10:197.
10. Hong H, et al. (2004) Aberrant expression of CARM1, a transcriptional coactivator of androgen receptor, in the development of prostate carcinoma and androgen-independent status. *Cancer* 101:83–89.
11. Osada S, et al. (2013) Elevated expression of coactivator-associated arginine methyltransferase 1 is associated with early hepatocarcinogenesis. *Oncol Rep* 30:1669–1674.
12. Cura V, Troffer-Charlier N, Wurtz JM, Bonnefond L, Cavarelli J (2014) Structural insight into arginine methylation by the mouse protein arginine methyltransferase 7: A zinc finger freezes the mimic of the dimeric state into a single active site. *Acta Crystallogr D Biol Crystallogr* 70:2401–2412.
13. van Haren M, van Ufford LQ, Moret EE, Martin NI (2015) Synthesis and evaluation of protein arginine N-methyltransferase inhibitors designed to simultaneously occupy both substrate binding sites. *Org Biomol Chem* 13:549–560.
14. Osborne T, Roska RL, Rajski SR, Thompson PR (2008) In situ generation of a bisubstrate analogue for protein arginine methyltransferase 1. *J Am Chem Soc* 130:4574–4575.
15. Troffer-Charlier N, Cura V, Hassenboehler P, Moras D, Cavarelli J (2007) Functional insights from structures of coactivator-associated arginine methyltransferase 1 domains. *EMBO J* 26:4391–4401.
16. Yue WW, Hassler M, Roe SM, Thompson-Vale V, Pearl LH (2007) Insights into histone code syntax from structural and biochemical studies of CARM1 methyltransferase. *EMBO J* 26:4402–4412.
17. Sack JS, et al. (2011) Structural basis for CARM1 inhibition by indole and pyrazole inhibitors. *Biochem J* 436:331–339.
18. Boriack-Sjodin PA, et al. (2016) Structural insights into ternary complex formation of human CARM1 with various substrates. *ACS Chem Biol* 11:763–771.
19. Lee J, Bedford MT (2002) PABP1 identified as an arginine methyltransferase substrate using high-density protein arrays. *EMBO Rep* 3:268–273.
20. Martin NI, Liskamp RM (2008) Preparation of N(G)-substituted L-arginine analogues suitable for solid phase peptide synthesis. *J Org Chem* 73:7849–7851.
21. Lakowski TM, 't Hart P, Ahern CA, Martin NI, Frankel A (2010) Nη-substituted arginyl peptide inhibitors of protein arginine N-methyltransferases. *ACS Chem Biol* 5:1053–1063.
22. 't Hart P, Lakowski TM, Thomas D, Frankel A, Martin NI (2011) Peptidic partial bisubstrates as inhibitors of the protein arginine N-methyltransferases. *Chembiochem* 12:1427–1432.
23. Troffer-Charlier N, Cura V, Hassenboehler P, Moras D, Cavarelli J (2007) Expression, purification, crystallization and preliminary crystallographic study of isolated modules of the mouse coactivator-associated arginine methyltransferase 1. *Acta Crystallogr Sect F Struct Biol Cryst Commun* 63:330–333.
24. Antonysamy S, et al. (2012) Crystal structure of the human PRMT5:MEP50 complex. *Proc Natl Acad Sci USA* 109:17960–17965.
25. Wang C, et al. (2014) Structural determinants for the strict monomethylation activity by trypanosoma brucei protein arginine methyltransferase 7. *Structure* 22:756–768.
26. Banerjee A, Yang W, Karplus M, Verdine GL (2005) Structure of a repair enzyme interrogating undamaged DNA elucidates recognition of damaged DNA. *Nature* 434:612–618.
27. Yang M, et al. (2007) Structural basis of histone demethylation by LSD1 revealed by suicide inactivation. *Nat Struct Mol Biol* 14:535–539.
28. Mailliot J (2013) Étude structurale de l'histonéméthyltransférase "CARM1" et de ses complexes biologiquement significatifs: Des structures 3D vers la conception rationnelle de composés à action pharmacologique. PhD thesis (University of Strasbourg, Strasbourg, France).
29. Bonnefond L, et al. (2015) Functional insights from high resolution structures of mouse protein arginine methyltransferase 6. *J Struct Biol* 191:175–183.
30. Vedadi M, et al. (2011) A chemical probe selectively inhibits G9a and GLP methyltransferase activity in cells. *Nat Chem Biol* 7:566–574.
31. Chen D, et al. (1999) Regulation of transcription by a protein methyltransferase. *Science* 284:2174–2177.
32. Kabsch W (2010) Xds. *Acta Crystallogr D Biol Crystallogr* 66:125–132.
33. Otwinowski Z, Minor W (1997) Processing of X-ray diffraction data collected in oscillation mode. *Methods Enzymol* 276:307–326.
34. Emsley P, Cowtan K (2004) Coot: Model-building tools for molecular graphics. *Acta Crystallogr D Biol Crystallogr* 60:2126–2132.
35. Adams PD, et al. (2010) PHENIX: A comprehensive Python-based system for macromolecular structure solution. *Acta Crystallogr D Biol Crystallogr* 66:213–221.
36. Winn MD, et al. (2011) Overview of the CCP4 suite and current developments. *Acta Crystallogr D Biol Crystallogr* 67:235–242.